ACS APPLIED MATERIALS & INTERFACES

Research Article

www.acsami.org

Highly Enhanced Acetone Sensing Performances of Porous and Single Crystalline ZnO Nanosheets: High Percentage of Exposed (100) Facets Working Together with Surface Modification with Pd Nanoparticles

Yuanhua Xiao,[†,‡] Lingzhen Lu,[†] Aiqin Zhang,[†] Yonghui Zhang,[†] Li Sun,[§] Lei Huo,[§] and Feng Li*[,†,‡,§]

[†]College of Materials and Chemical Engineering, State Laboratory of Surface and Interface Science and Technology, Zhengzhou University of Light Industry, Zhengzhou 450002, P. R. China

[‡]Institute of Applied Chemistry, Xinjiang University, Urumqi 820046, China

[§]The University of Texas, M. D. Anderson Cancer Center, Houston, Texas 77030, United States

Supporting Information

ABSTRACT: Porous and single crystalline ZnO nanosheets, which were synthesized by annealing hydrozincite $Zn_5(CO_3)_2(OH)_6$ nanoplates produced with a water/ethylene glycol solvothermal method, are used as building blocks to construct functional Pd−ZnO nanoarchitectures together with Pd nanoparticles based on a self-assembly approach. Chemical sensing performances of the ZnO nanosheets were investigated carefully before and after their surface modification with Pd nanoparticles. It was found that the chemical sensors made with porous ZnO nanosheets exhibit high selectivity and quick response for detecting acetone, because of the 2D ZnO nanocrystals exposed in (100) facets at high percentage. The performances of the acetone sensors can be further improved dramatically, after the surfaces of ZnO nanosheets are modified with Pd nanoparticles. Novel acetone sensors with enhanced response, selectivity and stability have been fabricated successfully by using nanoarchitectures consisting of ZnO nanosheets and Pd nanoparticles.

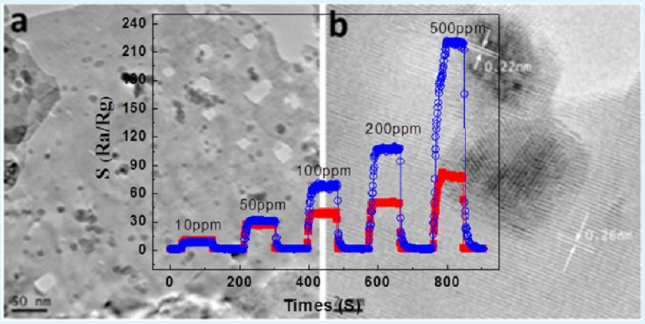

KEYWORDS: *ZnO nanosheets, Pd nanoparticles, nano-architectures, self-assembly, acetone sensors, enhanced performances*

INTRODUCTION

Acetone is an effective biomarker for noninvasive diagnosis of type-I diabetes because the disease causes the acetone concentration in human breath to increase from below 900 ppb for healthy individuals to higher than 1.8 ppm for type-I diabetes patients.[1] It is highly desirable to develop convenient and effective techniques for sensing acetone at low concentration. As one of the important semiconductor materials with a direct wide band gap of 3.37 eV, ZnO has been extensively investigated in the last decade. After they were first used as sensing materials to detect acetone in 1989,[2] ZnO nanocrystals including nanowires, nanorods, and nanoparticles have been used as building blocks in designing and constructing acetone sensors with improved sensing performances.[2−15] Recently, it was found that two dimensional (2D) ZnO nanosheets exhibit interesting gas sensing property.[12,16−20] ZnO nanowhiskers exposed in (001) facets, for instance, show improved responses for detecting ethanol in comparison to the ZnO nanowires exposed in (100) facets.[21] The composition, nanostructure and surface modification of semiconducting materials can dramatically affect their sensing performances.[22−29] Our researches on the design and fabrication of microdevices have also focused on preparation of nanocrystals for tailoring their functionalities.[30−34]

Because the surface modifications on semiconductor nanocrystals can change the interaction between oxygen absorbed on their surfaces and reducing gases,[35] nanoparticles of noble metal such as Pt, Au, and Pd have been attached onto the surface of semiconducting sensing materials to improve the response and selectivity of chemical sensors.[5,33,36] On the basis of a self-assembly technique, for instance, nanoarchitectures consisting of Pd nanoparticles and single crystalline ZnO nanowires were constructed successfully for fabricating H_2S sensors with highly improved responses, selectivity and stability.[33] After the surface modification with Au nanoparticles, ZnO nanowires show improved response to acetone.[5] Recently, it was found that Pd-doped ZnO nanofibers can monitor CO selectively, and Co-doped 1D ZnO nanocrystals can selectively detect ethanol, NO_2 and acetone.[37] To the best of our knowledge, however, there is no report in literature so far

Received: November 20, 2011
Accepted: August 1, 2012
Published: August 1, 2012

concerned with the surface modification of ZnO nanosheets with Pd nanoparticles and the investigation of their chemical sensing performances.

Herein, we report novel acetone sensors constructed with porous and single-crystalline ZnO nanosheets modified with Pd nanoparticles. Pre-made Pd nanoparticles can be uniformly attached onto the surfaces of ZnO nanosheets based on a self-assembly approach. The porous and single-crystalline ZnO nanosheets (ZnO−NSs), as well as the porous and single-crystalline ZnO nanosheets modified with Pd nanoparticles (Pd−ZnO−NSs), were used as sensing materials to fabricate acetone sensors, respectively. Initially, it was found that the 2D ZnO−NSs sandwiched in (100) facets of ZnO exhibit high response and selectivity for detecting acetone vapor. After further modification with Pd nanoparticles, Pd−ZnO−NSs exhibit highly improved acetone sensing performances including much higher response and stability, faster response and recovery, and lowered working temperature, compared to ZnO−NSs. It is interesting to find that the surface modification with Pd nanoparticles does not dramatically affect the selectivity of the acetone sensors fabricated. The porous structure of single crystalline ZnO nanosheets together with surface modification with Pd nanoparticles have resulted in excellent response and stability of acetone sensors working at lowered temperature, and the high acetone selectivity of the materials is dictated by the high percentage of exposed (100) facets of ZnO nanosheets.

EXPERIMENTAL SECTION

All of the reagents were analytically pure, and purchased from Shanghai Chemical Industrial Co. Ltd. (Shanghai, China), and used without further purification.

Synthesis of ZnO−NSs. The porous and single crystalline ZnO nanosheets were synthesized with a modified method described in the literature.[38] In a typical experiment, zinc acetate (2 mmol) and urea (4 mmol) were dissolved into pre-blended solution (40 ml) consisting of ethylene glycol and distilled water at a volume ratio of 1:1. After it was stirred for 15 min, the mixture was transferred into a Teflon-lined stainless steel autoclave and kept at 140 °C for 20 h. After the mixture was cooled to room temperature naturally, the precipitates were collected by centrifugation, thoroughly washed with deionized water and ethanol for 5 times each, and dried in an oven at 70 °C for 12 h to get white powders of hydrozincite $Zn_5(CO_3)_2(OH)_6$ precursor with a yield of 85%. The precursor was finally calcined at 400 °C for 2 h to produce white ZnO nanosheets in large scale.

Synthesis of Pd Nanoparticles. The Pd nanoparticles were synthesized following the method reported by Xia group.[39] In a typical synthesis, ethylene glycol (EG, 5 ml) was placed in a 3-neck flask equipped with a reflux condenser and a magnetic Teflon-coated stirring bar and heated in air at 110 °C for 1 h. Meanwhile, Na_2PdCl_4 (0.1384 g) and PVP (K-30, 0.0800 g) were separately dissolved in EG (3 ml) at room temperature. Then, the two solutions were injected simultaneously into the flask. After that, the mixture solution was maintained at 110 °C for 9 h. The samples were washed with acetone and then with ethanol for several times by centrifugation.

Surface Modification of ZnO Nanosheets with Pd Nanoparticles. The surfaces of ZnO−NSs were modified with Pd nanoparticles with a self-assembly approach developed in our labs.[33] Briefly, colloid solution of Pd nanoparticles in water was added into an agate mortar with ZnO nanosheets (20.0 mg), and the mixture was then ground and subsequently annealed at 600 °C for 2 h to obtain grey powders loaded with Pd nanoparticles of 0.2, 0.5, and 1.0 wt %.

Materials Characterization. The crystal structures of the as-prepared products were characterized by powder X-ray diffraction (XRD) on a D/max 2550 V X-ray diffractometer (Rigaku, Tokyo, Japan) with monochromatized Cu Kα radiation (λ = 1.54056 Å; scanning rate = 0.04° s^{-1} in the range of 10−80°) incident radiation. Morphologies and sizes of all products were analyzed with Field Emission Scanning Electron Microscopy (FESEM, JEOL, JSM-7001F, 10 kV) and Transmission Electron Microscopy (TEM, JEOL, JEM-2100 operated at 200 kV). The elemental analyses were investigated by energy-dispersive X-ray micro-analyzer (EDS), which was embedded in the JEM-2100 microscope. High-resolution transmission electron microscope images (HRTEM) and selective area electron diffraction pattern (SAED) were characterized using JEM-2100 microscope. In the preparation of samples for TEM observation, the materials were first dispersed in ethanol using an ultrasonic bath and then dropped onto a cupper grid, which was dried in air at room temperature and kept in vacuum for 20 min before TEM observation. The specific surface area was measured using a ST-2000 surface area and pore size analyzer (Quantachrome Instruments). The pore size distribution was determined using the BJH method applied to the desorption branch of adsorption-desorption isotherms.

Fabrication of Chemical Sensors. The chemical sensors were fabricated with as-synthesized samples as sensing materials. The materials were dispersed into adhesive Terpineol through gently grinding in an agate mortar to form a slurry suspension. The paste was then coated onto the surfaces of ceramic tubes with two Pt electrodes. The elements coated with sensing materials were subsequently dried at 80 °C and calcined at 500 °C for 1 h to produce thick films on the surfaces. No conductive binder was added into the materials. A small Ni−Cr alloy coil was finally inserted into the tube as a heater for controlling the working temperature to obtain side-heating type devices. The elements were further aged at 300 °C for 7 days to improve the stability before testing. Three elements were fabricated with each of ZnO−NSs and Pd−ZnO−NSs, respectively, to investigate the stability of the sensors. The gas sensing properties of the elements fabricated were measured using a static test system made by Hanwei Electronics Co. Ltd., Henan Province, China. For reducing gases, which decreases the resistance of chemical sensors constructed with N-type semiconductor sensing materials, the response is defined as response = R_a/R_g, where Ra is the sensor resistance in air and R_g is the resistance in gases tested. The relative humidity of the testing atmosphere is about 25%. The response time is defined as the time required for the variation in conductance to reach 90% of the equilibrium value after injecting a test gas, and the recovery time is defined as the time necessary for the sensor to return to 10% above the original conductance in air after releasing the test gas.

RESULTS AND DISCUSION

Because nanosized materials may exhibit functionalities corresponding to their nanostructures encased in specific facets,[24] it is expected that the ZnO nanosheets exposed in specific facets and their composites with Pd nanoparticles could show highly enhanced gas sensing behaviors. In order to investigate the effect of 2D nanostructure on the gas sensing functionalities of ZnO nanocrystals, we first synthesized ZnO nanosheets based on a solvothermal reaction method. The as-prepared white powders in solvothermal reaction were characterized with XRD to verify their structure. All of the diffraction peaks as shown in Figure 1a can be indexed as hydrozincite $Zn_5(CO_3)_2(OH)_6$ (JCPDS Card No.19-1458). The results indicate that a hydrozincite precursor has been produced in the solvothermal reaction. After annealed at 400 °C for 2 h, the precursor has completely transformed from hydrozincite $Zn_5(CO_3)_2(OH)_6$ into hexagonal ZnO phase (eq 1) as shown in Figure 1b. The sharp reflection peaks of the XRD patterns suggest that the precursor and final ZnO product (JCPDS card No. 79-2205) are of highly crystalline. There is no other diffraction peaks detected (5% deviation), which indicates that no impurity exists in the final product.

$$Zn_5(CO_3)_2(OH)_6(s) \rightarrow 5ZnO(s) + 2CO_2(g) + 3H_2O(g) \quad (1)$$

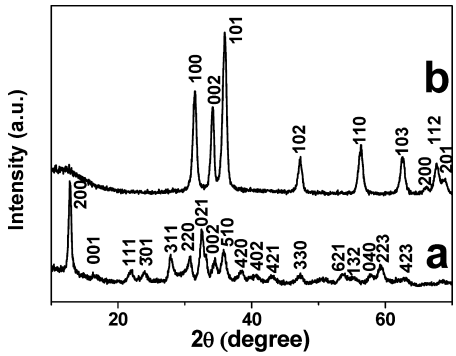

Figure 1. XRD patterns of (a) hydrozincite $Zn_5(CO_3)_2(OH)_6$ produced in solvothermal reactions and (b) ZnO powers after annealed at 400 °C for 2 h.

The morphologies of $Zn_5(CO_3)_2(OH)_6$ and the final ZnO products were carefully investigated with FESEM. Figure 2a shows a typical FESEM image of the precursor. 2D nanosheets of a few to tens micrometer in dimension with smooth surfaces have been produced in large scale. The thickness of $Zn_5(CO_3)_2(OH)_6$ nanosheets is about 15.1 nm (Figure 2b). After annealed at 400 °C, the final ZnO products as shown in Figure 2c and d still maintain uniform 2D sheet-like morphology of the precursor. The edge thickness of the 2D ZnO nanosheets shrinks to about 13.5 nm. Compared to the smooth surface of the precursor, however, a lot of nanosized pores have been generated across the 2D ZnO nanosheets. The porous structure on the surfaces of ZnO nanosheets should be resulted from the decomposition of hydrozincite $Zn_5(CO_3)_2(OH)_6$ and the subsequent release of H_2O and CO_2 from the precursor (eq 1). The final ZnO products from hydrozincite $Zn_5(CO_3)_2(OH)_6$ nanosheets have inherited the 2D nanostructure of the precursor.

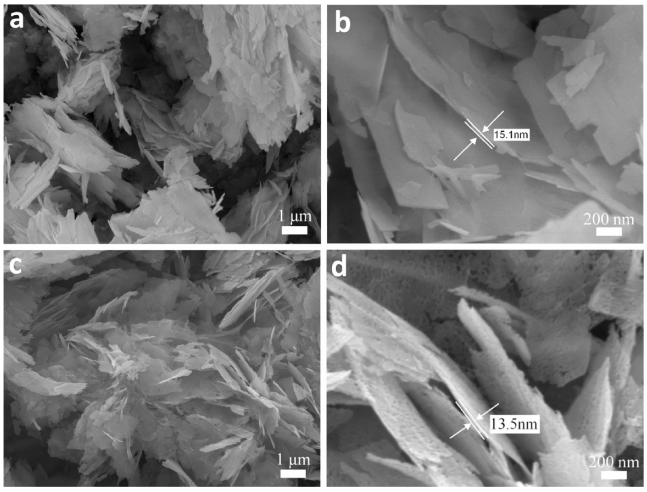

Figure 2. FESEM images of (a,b) hydrozincite $Zn_5(CO_3)_2(OH)_6$ and (c,d) porous ZnO nanosheets.

The microstructure of the porous ZnO nanosheets was further investigated in detail by TEM and SAED. Figure 3a shows the typical TEM image of one ZnO nanosheet. Nanosized pores of a few to tens nanometers in diameter can be observed clearly across nanosheets of about 1 μm in dimension. It is interesting to find that the SAED pattern (inset in Figure 3a, Supporting Information Figure S1) corresponding to the whole porous ZnO nanosheet as shown in Figure 3a consists of well ordered dots. Porous and single crystalline ZnO nanosheets (assigned to ZnO−NSs) have been produced successfully after annealing hydrozincite at 400 °C. The HRTEM image (Figure 3b)further confirms the single crystalline feature of the ZnO−NSs. The d-spacing of 0.26 nm of the lattice fringes corresponds to the (002) plane of the hexagonal structure of ZnO. The 2D ZnO nanosheets have been sandwiched by their two (100) planes. A pore with irregular shape of about 12 nm in diameter is also highlighted at the center of the HRTEM image.

The porous feature of ZnO−NSs was further confirmed by BET analysis. Figure 4 shows the N_2 adsorption−desorption isotherm and the corresponding BJH pore size distribution (inset in Figure 4) of the porous nanosheets. According to the IUPAC classification,[40] the loop observed is ascribed as type H3 loops, indicating the existence of abundant pores of 2−50 nm in diameter. While the size and shape of the pores were not uniform, most of them are around 7 nm in diameter (pore volume: 0.13 cm^3/g) and the average pore diameter is ~22 nm. The results are consistent with those obtained from TEM observation. The BET surface area of the material is 91.93 m^2/g.

To fabricate chemical sensors with enhanced performances, we further adopted a self-assembly approach developed by our lab to modify the surfaces of ZnO−NSs.[33] Figure 5a shows TEM image of ZnO nanosheets modified with 0.5 wt % Pd nanoparticles. In addition to the pores on the smooth surface of

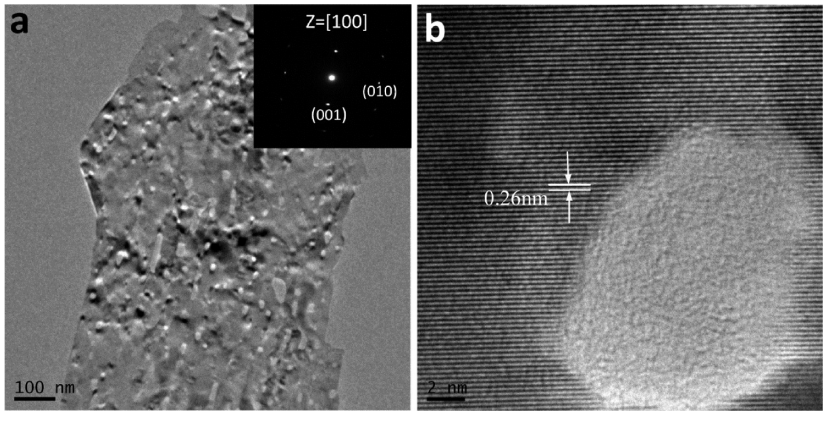

Figure 3. (a) TEM image and (b) HRTEM image of ZnO−NSs. The inset in panel a shows the SAED patterns of the porous nanosheet.

dx.doi.org/10.1021/am3010303 | ACS Appl. Mater. Interfaces 2012, 4, 3797−3804

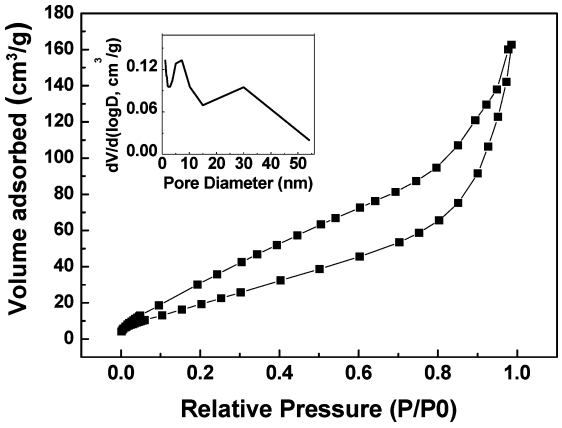

Figure 4. Typical nitrogen adsorption−desorption isotherm and pore-size distribution curve (inset) of ZnO−NSs.

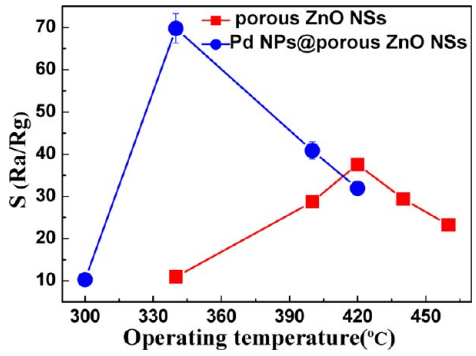

Figure 6. Responses to 100 ppm acetone versus operating temperature of acetone sensors made with porous and single-crystalline ZnO nanosheets and Pd-modified ZnO nanosheets.

nanosheets, many circular black dots of ∼8 nm in diameters are clearly observed uniformly attaching onto the nanosheet surfaces. The HRTEM image of the nanoarchitecture as shown in Figure 5b reveals that Pd nanoparticles have been closely attached onto the surface of ZnO nanosheets. The lattice spacing measurements give recurrent values of 0.22 and 0.26 nm, which correspond to the (111) plane of metallic Pd phase and (002) facet of ZnO nanosheets, respectively. Defect and steps can also be observed around the interface between Pd nanoparticles and the ZnO nanosheets. The energy-dispersive X-ray spectroscopy (EDS) analysis (inset in Figure 5b) further confirms that the nanosheets with black dots are composed of Zn, Pd, and O. The peaks corresponding to Cu come from Cu grids. Porous and single crystalline ZnO nanosheets modified with Pd nanoparticles (assigned to Pd−ZnO−NSs) have been successfully fabricated based on self-assembly of Pd nanoparticles of the surfaces of ZnO nanosheets.

Based on as-prepared 2D nanosheets (ZnO−NSs and Pd−ZnO-NSs), we fabricated chemical sensors and investigated their gas sensing performances. Figure 6 shows the responses via temperature curves of acetone sensors made with ZnO−NSs and Pd−ZnO−NSs, respectively. The responses of the sensors to acetone vary dramatically from 200 to 500 °C. The ZnO−NSs sensors reach to their maximum response of 37.5 to 100 ppm acetone when elevating the operating temperature to 420 °C, and their responses then decrease after further increasing the temperature. The optimal operating temperature of the ZnO−NSs sensors is 420 °C. The response of our ZnO−NSs is higher than that of acetone sensors made with multilayered ZnO nanosheets reported recently,[12,17] as well as that of the acetone sensors from dumbbell-like ZnO nanocrystals.[4] The acetone sensing performances of ZnO−NSs sensors is also much better than that of sensors constructed from ZnO thin films[6] and ZnO quantum dot embedded in polyvinyl pyrrolidone.[10] In addition, ZnO−NSs sensors show higher response than acetone sensor fabricated with WO_3 nanoparticles[41] and other materials including Fe_2O_3,[42] In_2O_3,[43] TiO_2,[44] CeO_2,[45] perovskite oxide,[46] and ferrites.[47]

After the surface modification with Pd nanoparticles (0.5 wt %), the maximum response of the sensors made with Pd−ZnO−NSs jumps to 70.0 working at the optimized operating temperature of 340 °C as shown in Figure 6. The acetone response of Pd−ZnO−NSs sensor is approximately one time higher than that of ZnO−NSs sensors, and approximately ten times higher than that of our acetone sensors made with SnO_2 nanowires encased in (100) facets.[32] It is also about 100 times higher than that of acetone sensors fabricated with ZnO fibers modified with Pd nanoparticles,[48] and more than 4 times higher than that from Co-doped ZnO fibers.[11] Our acetone sensors also show much better response, compared to Au modified ZnO nanowire sensors.[5] The response of Pd−ZnO−NSS sensors is comparable to that of acetone sensors made with Si-doped WO_3 nanoparticles.[49] The optimal operating temper-

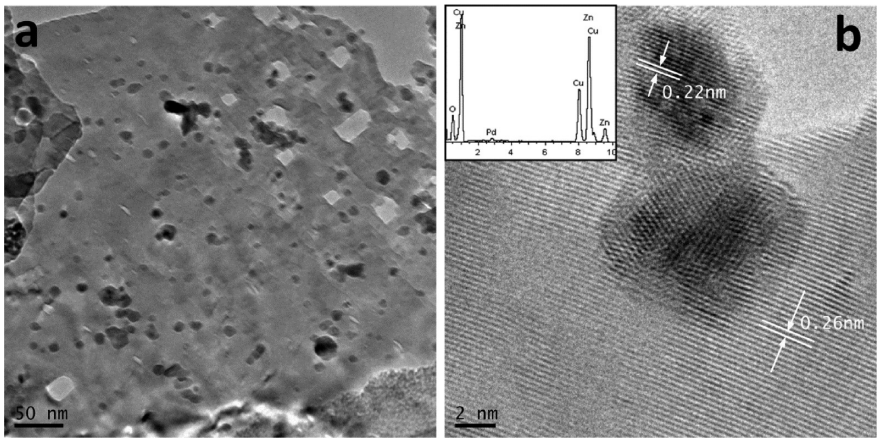

Figure 5. (a) TEM image and (b) HR-TEM image of Pd nanoparticles@ZnO NSs. The inset in panel b shows EDS of the nanosheets.

ature of Pd−ZnO−NSs sensors is also lowered to 340 °C from 420 °C of the ZnO−NSs sensors, which is also lower than that of Co-doped ZnO fibers.[11] Supporting Information Figure S2 shows the dynamic responses and the responses vs. concentration curves of the sensors made with Pd−ZnO−NSS loaded with Pd nanoparticles ranging from 0.2 wt % to 1.0 wt %. Table 1 presents the effect of the amount of Pd nanoparticles attached onto the surfaces of ZnO nanosheets on the responses of acetone sensors. The optimal amount of Pd nanoparticles is 0.5 wt %.

Table 1. Effect of Pd Nanoparticles on the Responses of Sensors to Acetone of 100 ppm

amount of Pd nanoparticles	0.0 wt %	0.2 wt %	0.5 wt %	1.0 wt %
responses	37.5	42.2	70.0	40.8

Figure 7a shows the dynamic response and recovery of sensors made with ZnO−NSs and Pd−ZnO−NSs. It can be clearly observed that the Pd−ZnO−NSs sensors exhibit much higher responses to acetone of concentrations higher than 100 ppm in comparison with ZnO−NSs sensors. The sensors made with Pd−ZnO−NSs are able to achieve a response of ~222 to acetone of 500 ppm, which is almost 3 times higher than that of ZnO−NSs sensors. The response and recovery times of Pd−ZnO−NSs sensors to acetone of 100 ppm also decrease to 9 and 6 s, respectively, compared to that of 10 and 7 s of ZnO−NSs sensors. However, the response difference between the two types of acetone sensors diminishes with decreasing acetone concentrations. There is no big difference in their responses to acetone after the acetone concentration is lowered to 50 ppm. The highly enhanced response of the sensors may be resulted from the specific porous structure of ZnO nanosheets and their surface modification with Pd nanoparticles. The porous structure can greatly facilitate gas diffusion and mass transportation in a manner similar to ZnO nanoparticles and thus improve the sensors' response to the chemicals detected. In addition, the ethanol response of the Pd−ZnO−NSs sensors (Figure 7c) is also increased dramatically after attaching Pd nanoparticles onto the surfaces of ZnO nanosheets. Acetone sensors with highly enhanced response can be fabricated by using ZnO nanosheets modified with Pd nanoparticles as sensing materials.

It was found that the main drawback of chemical sensors made with ZnO nanocrystals is their low working stability.[23] We have carefully investigated the long term performances of our sensors and found that the acetone sensors made with Pd−ZnO−NSs exhibit highly improved stability, as shown in Figure 7b, compared to ZnO−NSs sensors. After running for 60 days, the responses of Pd−ZnO−NSs sensors to acetone of 100 ppm maintain at ~70. Compared to the response decrease from 37.5 to 26.5, which is about 30.4% for the ZnO−NSs sensor in 60 days, the stability of Pd−ZnO−NSs sensors has been improved dramatically. In addition, the dynamic responses of four acetone sensors made with Pd−ZnO−NSs as shown in Supporting Information Figure S3 can further verify their excellent performances. The much better stability of the sensors made with Pd−ZnO−NSs may be resulted from the stable structure of single crystalline ZnO nanosheets and lowered working temperature by attaching Pd nanoparticles onto their surfaces.[50] The sensors made with porous and single crystalline ZnO nanosheets modified with Pd nanoparticles have the

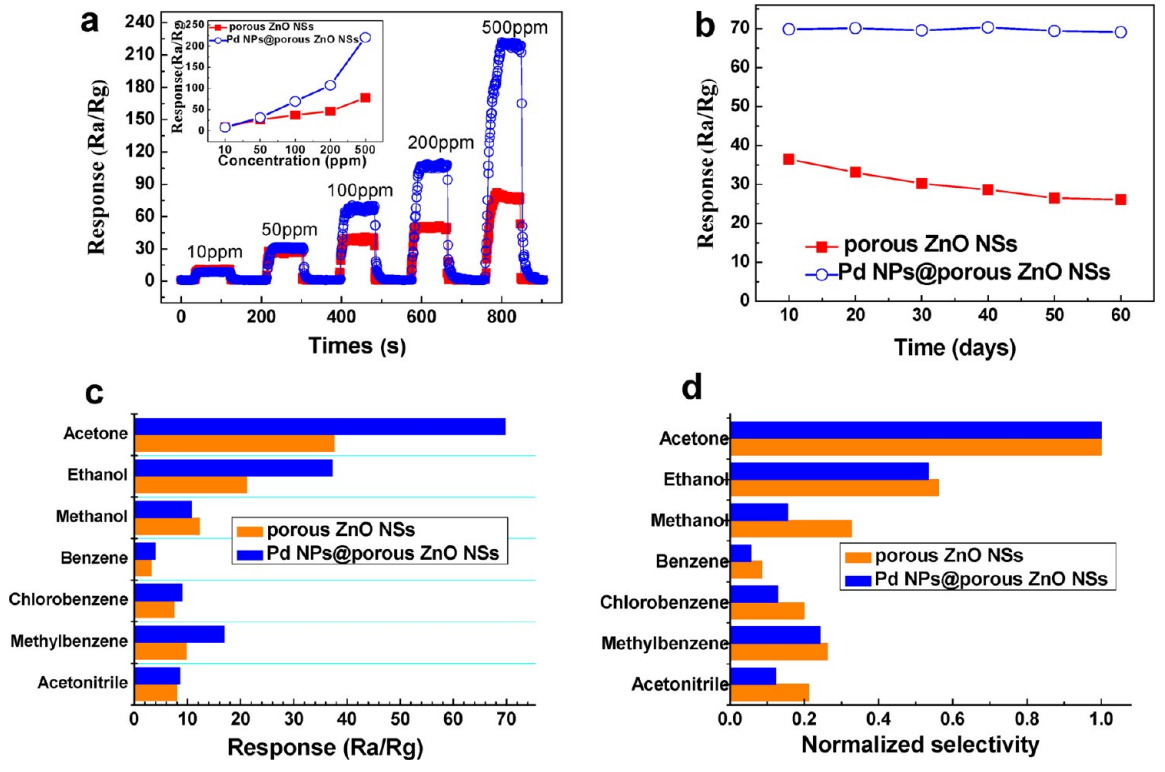

Figure 7. (a) Dynamic responses to acetone at concentrations ranging from 10 to 500 ppm of acetone sensors made with Pd−ZnO−NSs and ZnO−NSs at optimized operating temperatures. The inset shows response via concentration curves of the corresponding sensors. (b) The stability studies of sensors exposed to acetone of 100 ppm. (c) The selectivity of the acetone sensors to reducing gases tested, and (d) the corresponding normalized selectivity of sensors from (c).

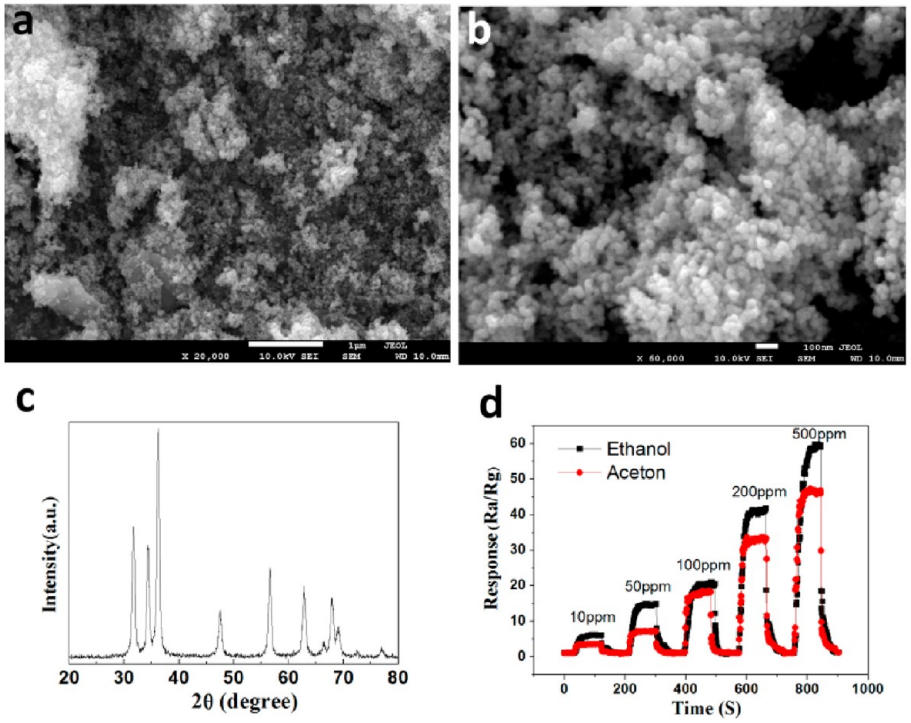

Figure 8. (a,b) FESEM images of ZnO nanoparticles of 40 nm in diameter. (c) XRD pattern of ZnO nanoparticles. (d) Dynamic responses to ethanol and acetone of sensors made with ZnO nanoparticles.

advantages of sensors made with ZnO nanowires and nanoparticles, which show high stability and the high response, respectively. The high stability of acetone sensors fabricated with Pd−ZnO−NSs could be attributed to the single crystalline feature of ZnO nanosheets and the lowered working temperature.

Because the specific facets of semiconductor nanocrystals could exhibit selective adsorption to specific gas molecules, metal oxide nanocrystals may show tunable gas sensing properties depending on their exposed crystal facets.[24,32] We thus fabricated two gas sensors with Pd−ZnO−NSs and ZnO−NSs as sensing materials, respectively, for investigating their performances in selectivity. All of the sensors were tested with reducing gases at concentration of 100 ppm and at the optimal operating temperature. Figure 7c shows the responses of these sensors to reducing gases including acetone, ethanol, methanol, benzene, chlorobenzene, methylbenzene, and acetonitrile. Based on the responses as shown in Figure 7c, it is very clear to discover that both sensors made with Pd−ZnO−NSs and ZnO−NSs exhibit the highest responses to acetone in comparison to their responses to other gases. To accurately compare the selectivity of the sensors, the results as shown in Figure 1c is further normalized and presented again in Figure 7d. It is clear as shown in Figure 7d that both sensors demonstrate the highest selectivity to acetone, compared to that of other gases detected. In addition, the ethanol response of the Pd−ZnO−NSs sensors increased dramatically, after attaching Pd nanoparticles onto the surfaces of ZnO nanosheets. The ethanol response of Pd−ZnO−NSs sensors is also much higher than that of ethanol sensors fabricated with ZnO nanosheets modified with Au nanoparticles.[19] After the surfaces of ZnO−NSs were modified with Pd nanoparticles; however, the response ratio of the sensors to acetone and ethanol has only been improved slightly from 1.8 to 1.9. The selectivity changes of Pd−ZnO−NSs sensors are relatively small in comparison with their highly enhanced response to acetone (Figure 7c).

Recently, it was found that 2D nanocrystals exhibit interesting functionalities including catalysis, energy storage, and gas sensing properties,[24,31b,51] and ZnO nanocrystals can detect acetone selectively.[12,17] The computer simulation also revealed that ZnO nanosheets exposed in (100) facets exhibit much higher interaction with NO_2 and NO.[52] It is critical to understand the sensing mechanism for designing acetone sensors of high sensing performances. If we take a square-shaped nanosheet with edges of 1 μm in length as an example, a simple and rough calculation indicates that a smooth nanosheet of 13.5 nm in thickness will be sandwiched in (100) facets at a very high percentage of ~96.9%. Based on the SEM and TEM observations of single crystalline ZnO nanosheets prepared in this work, we can find that their dimensions are in the range of several to tens of micrometers and the pore density on their surfaces is ~162 pores/μm^2. While there are pores of irregular shapes on their surfaces, the majority of the specific surface area of the materials should be contributed by the (100) facets of ZnO nanosheets, which could have led to the excellent acetone sensing performances of the materials.

To further investigate the structure effect of ZnO nanosheets on their gas sensing performances, ZnO nanoparticles of ~40 nm were synthesized and used as sensing materials to construct chemical sensors as control. The morphology and composition of the nanoparticles are characterized with FESEM (Figure 8a and b) and XRD (Figure 8c). The dynamic responses of the ZnO nanoparticles sensors as shown in Figure 8d clearly reveal that devices show higher sensitivities to ethanol, compared to their responses to acetone. This indicates that the ZnO nanoparticles sensors exhibit much less selectivity to acetone in comparison to that of ZnO−NSs and ZnO−Pd−NSs sensors. The sensitivities to both ethanol and acetone of sensors made with the ZnO nanoparticles are also much lower than that of

those fabricated with ZnO NSs and ZnO−Pd−NSs. The results clearly reveal the 2D structure effect of porous ZnO nanosheets on their gas sensing functionalities including sensitivity and selectivity. It is thus safe for us to conclude that the high selectivity of ZnO−NSs sensors has been aroused by the exposed (100) facets of ZnO nanosheets, which could absorb acetone molecules onto their surfaces selectively. The interaction between the (100) facets of ZnO nanosheets and the acetone molecules could be only changed slightly by the surface modification of the nanosheets with Pd nanoparticles. This may have led to that the two sensors both made with ZnO nanosheets, regardless of whether receiving surface modification with Pd nanoparticles, exhibit similar high selectivity to acetone.

For chemical sensors based on semiconductor materials, it is well accepted that the formation of oxygen adsorption induced electron depletion layer on their surfaces plays an important role in the sensing response of gas sensors.[35] After closely attached onto the surfaces of ZnO nanocrystals, Pd nanoparticles can form Schottky barrier-type junctions together with ZnO,[53] which result in the change of the electron depletion layer near the interface of ZnO nanocrystals and Pd nanoparticles. In addition, Pd nanoparticles can enhance the catalytic dissociation of the molecular absorbed on the surfaces of semiconductor nanocrystals and result in the produced atomic species on their surfaces diffusing at lowered working temperature.[54] Novel sensors with highly enhanced response and stability can thus be fabricated with porous and single crystalline ZnO nanosheets modified with Pd nanoparticles on surface. The computer simulation to further understand the gas sensing performances of ZnO nanosheets is on the way in our lab and the results will be reported in the future.

CONCLUSION

In summary, acetone sensors were fabricated successfully with porous and single-crystalline ZnO nanosheets modified with Pd nanoparticles as sensing materials. It was found that Pd-ZnO-NSs sensors exhibit highly enhanced stability and response to acetone. The results also indicate that the single crystalline ZnO nanostructures encased in specific (100) facets exhibit their effect on the selectivity of acetone sensors. The availability of diverse 2D and 3D ZnO nanocrystals encased in high index facets could enable us to improve the sensing performances of chemical sensors dramatically and to open a new pathway for designing novel acetone sensors.

ASSOCIATED CONTENT

Supporting Information

Additional TEM Image at low magnification and corresponding SAED patterns; the dynamic responses of acetone sensors made with Pd−ZnO−NSs loaded with different amount of Pd nanoparticles; responses of sensors loaded with different amount of Pd nanoparticles to acetone of different concentrations; dynamic responses of additional four sensors to acetone of different concentrations. This material is available free of charge via the Internet at http://pubs.acs.org/.

AUTHOR INFORMATION

Corresponding Author

*E-mail: lifeng696@yahoo.com; fengli@zzuli.edu.cn. Fax: 86-371-6355-6510. Tel: 86-371-6355-6510.

Notes

The authors declare no competing financial interest.

ACKNOWLEDGMENTS

The authors are grateful to the financial support from the National Natural Science Foundation of China (NSFC. 21071130 and 21141005), Outstanding Scholar Program of Henan Province (114200510012), Key Program of Henan Province for Science and Technology (112102210239 and 92102310334). Thanks must be given to Dongming Li at UT Southwestern Medical Center for his comments to this paper.

REFERENCES

(1) Wang, L.; Teleki, A.; Pratsinis, S. E.; Gouma, P. I. *Chem. Mater.* **2008**, *20*, 4794.
(2) Reichel, J.; Seyffarth, T.; Guth, U.; Mobius, H. H.; Gockeritz, D. *Pharmazie* **1989**, *44*, 698.
(3) Zeng, Y.; Zhang, T.; Yuan, M. X.; Kang, M. H.; Lu, G. Y.; Wang, R.; Fan, H. T.; He, Y.; Yang, H. B. *Sens. Actuators B* **2009**, *143*, 93.
(4) Qi, Q.; Zhang, T.; Liu, L.; Zheng, X. J.; Yu, Q. J.; Zeng, Y.; Yang, H. B. *Sens. Actuators B* **2008**, *134*, 166.
(5) Chang, S. J.; Hsueh, T. J.; Chen, I. C.; Hsieh, S. F.; Chang, S. P.; Hsu, C. L.; Lin, Y. R.; Huang, B. R. *IEEE Trans. Nanotechnol.* **2008**, *7*, 754.
(6) Sahay, P. P. *J. Mater. Sci.* **2005**, *40*, 4383.
(7) Anno, Y.; Maekawa, T.; Tamaki, J.; Asano, Y.; Hayashi, K.; Miura, N.; Yamazoe, N. *Sens. Actuators B* **1995**, *25*, 623.
(8) Vohs, J. M.; Barteau, M. A. *J. Phys. Chem.* **1991**, *95*, 297.
(9) Wetchakun, K.; Siriwong, C.; Liewhiran, C.; Wisitsoraat, A.; Phanichphant, S. *Sens. Lett.* **2011**, *9*, 299.
(10) Nath, S. S.; Choudhury, M.; Chakdar, D.; Gope, G.; Nath, R. K. *Sens. Actuators B* **2010**, *148*, 353.
(11) Liu, L.; Li, S. C.; Zhuang, J.; Wang, L. Y.; Zhang, J. B.; Li, H. Y.; Liu, Z.; Han, Y.; Jiang, X. X.; Zhang, P. *Sens. Actuators B* **2011**, *155*, 782.
(12) Li, J.; Fan, H. Q.; Jia, X. H. *J. Phys. Chem. C* **2010**, *114*, 14684.
(13) Li, B.; Liu, S. Q.; Liu, L.; Cui, Y. M.; Guo, X. F.; Zhou, X. F. *Chin. J. Inorg. Chem.* **2010**, *26*, 591.
(14) Gong, J.; Li, Y. H.; Chai, X. S.; Hu, Z. S.; Deng, Y. L. *J. Phys. Chem. C* **2010**, *114*, 1293.
(15) Choudhury, M.; Nath, S. S.; Chakdar, D.; Gope, G.; Nath, R. K. *Adv. Sci. Lett.* **2010**, *3*, 6.
(16) Jing, Z. H.; Zhan, J. H. *Adv. Mater.* **2008**, *20*, 4547.
(17) Fan, H. Q.; Jia, X. H. *Solid State Ionics* **2011**, *192*, 688.
(18) Liu, Y.; Dong, J.; Hesketh, P. J.; Liu, M. L. *J. Mater. Chem.* **2005**, *15*, 2316.
(19) Liu, X. H.; Zhang, J.; Wang, L. W.; Yang, T. L.; Guo, X. Z.; Wu, S. H.; Wang, S. R. *J. Mater. Chem.* **2011**, *21*, 349.
(20) Liu, J. Y.; Guo, Z.; Meng, F. L.; Luo, T.; Li, M. Q.; Liu, J. H. *Nanotechnology* **2009**, *20*, 125501.
(21) Liu, J.; Chen, X. L.; Wang, W. J.; Liu, Y.; Huang, Q. S.; Guo, Z. P. *Cryst. Eng. Comm.* **2011**, *13*, 3425.
(22) Gurlo, A. *Nanoscale* **2010**, *3*, 154.
(23) Polarz, S.; Roy, A.; Lehmann, M.; Driess, M.; Kruis, F. E.; Hoffmann, A.; Zimmer, P. *Adv. Funct. Mater.* **2007**, *17*, 1385.
(24) Han, X. G.; Jin, M. S.; Xie, S. F.; Kuang, Q.; Jiang, Z. Y.; Jiang, Y. Q.; Xie, Z. X.; Zheng, L. S. *Angew. Chem. Int. Ed.* **2009**, *48*, 9180.
(25) Zhang, W.-D.; Zhang, W.-H.; Ma, X.-Y. *J. Mater. Sci.* **2009**, *44*, 4677.
(26) Kim, K.-M.; Kim, H.-R.; Choi, K.-I.; Kim, H.-J.; Lee, J.-H. *Sens. Actuators B* **2011**, *155*, 745.
(27) Huang, J; Wu, Y.; Gu, C.; Zhai, M.; Yu, K.; Yang, M.; Liu, J. *Sens. Actuators B* **2010**, *146*, 206.
(28) Jia, X.; Fan, H. *Mater. Lett.* **2010**, *64*, 1574.
(29) Feng, P.; Wan, Q.; Wang, T. H. *Appl. Phys. Lett.* **2005**, *87*, 213111.
(30) Xiao, Y.; Liu, S.; Fang, S.; Jia, D.; Su, H.; Zhou, W.; Wiley, J.; Li, F. *RSC Adv.* **2012**, *2*, 3496.

(31) (a) Xiao, Y.; Liu, S.; Li, F.; Zhang, A.; Zhao, J.; Fang, S.; Jia, D. *Adv. Funct. Mater.* **2012**, DOI: 10.1002/adfm.201200519. (b) Xiao, Y.; Zhang, A.; Liu, S.; Zhao, J.; Fang, S.; Jia, D.; Li, F. *J. Power Sources* **2012**, DOI: 10.1016/j.jpowsour.2012.07.030.
(32) Qin, L. P.; Xu, J. Q.; Dong, X. W.; Pan, Q. Y.; Cheng, Z. X.; Xiang, Q.; Li, F. *Nanotechnology* **2008**, *19*, 185705.
(33) Zhang, Y.; Xiang, Q.; Xu, J. Q.; Xu, P. C.; Pan, Q. Y.; Li, F. *J. Mater. Chem.* **2009**, *19*, 4701.
(34) Li, F.; Ding, Y.; Gao, P. X. X.; Xin, X. Q.; Wang, Z. L. *Angew. Chem. Int. Ed.* **2004**, *43*, 5238.
(35) Yamazoe, N.; Sakai, G.; Shimanoe, K. *Catal. Surv. Asia* **2003**, *7*, 63.
(36) von Wenckstern, H.; Biehne, G.; Rahman, R. A.; Hochmuth, H.; Lorenz, M.; Grundmann, M. *Appl. Phys. Lett.* **2006**, *88*, 092102.
(37) Na, C. W.; Woo, H. S.; Kim, I. D.; Lee, J. H. *Chem. Commun.* **2011**, *47*, 5148.
(38) Wang, X. B.; Cai, W. P.; Lin, Y. X.; Wang, G. Z.; Liang, C. H. *J. Mater. Chem.* **2010**, *20*, 8582.
(39) Xiong, Y. J.; Chen, J. Y.; Wiley, B.; Xia, Y. N. *J. Am. Chem. Soc.* **2005**, *127*, 7332.
(40) Sing, K.; Everett, D.; Haul, R.; Moscou, L.; Pierotti, R.; Rouquerol, J.; Siemieniewska, T. *Pure Appl. Chem.* **1985**, *57*, 603.
(41) Khadayate, R. S.; Sali, V.; Patil, P. P. *Talanta* **2007**, *72*, 1077.
(42) Wang, S. R.; Wang, L. W.; Yang, T. L.; Liu, X. H.; Zhang, J.; Zhu, B. L.; Zhang, S. M.; Huang, W. P.; Wu, S. H. *J. Solid State Chem.* **2010**, *183*, 2869.
(43) Neri, G.; Bonavita, A.; Micali, G.; Donato, N. *IEEE Sens. J.* **2010**, *10*, 131.
(44) Rella, R.; Spadavecchia, J.; Manera, M. G.; Capone, S.; Taurino, A.; Martino, M.; Caricato, A. P.; Tunno, T. *Sens. Actuators B* **2007**, *127*, 426.
(45) Bene, R.; Perczel, I. V.; Reti, F.; Meyer, F. A.; Fleisher, M.; Meixner, H. *Sens. Actuators B* **2000**, *71*, 36.
(46) Murade, P. A.; Sangawar, V. S.; Chaudhari, G. N.; Kapse, V. D.; Bajpeyee, A. U. *Curr. Appl. Phys.* **2010**, *11*, 451.
(47) Rezlescu, N.; Iftimie, N.; Rezlescu, E.; Doroftei, C.; Popa, P. D. *Sens. Actuators B* **2006**, *114*, 427.
(48) Wei, S. H.; Yu, Y.; Zhou, M. H. *Mater. Lett.* **2010**, *64*, 2284.
(49) Righettoni, M.; Tricoli, A.; Pratsinis, S. E. *Anal. Chem.* **2011**, *82*, 3581.
(50) Xing, L. L.; Ma, C. H.; Chen, Z. H.; Chen, Y. J.; Xue, X. Y. *Nanotechnology* **2011**, *22*, 215501.
(51) McLaren, A.; Valdes-Solis, T.; Li, G. Q.; Tsang, S. C. *J. Am. Chem. Soc.* **2009**, *131*, 12540.
(52) Breedon, M.; Spencer, M. J. S.; Yarovsky, I. *J. Phys. Chem. C* **2011**, *114*, 16603.
(53) Xu, J. H.; Wu, N. Q.; Jiang, C. B.; Zhao, M. H.; Li, J.; Wei, Y. G.; Mao, S. X. *Small* **2006**, *2*, 1458.
(54) Lee, Y. C.; Huang, H.; Tan, O. K.; Tse, M. S. *Sens. Actuators B* **2008**, *132*, 239.